Vladimir Divić
Ivana Uzelac
Bernardin Peroš

ISSN 1333-1124
eISSN 1849-1391

MULTIPLICATIVE DECOMPOSITION BASED FDEM MODEL FOR MEMBRANE STRUCTURES

UDC 624.04.074.4:004.42.738.5

Summary

A finite strain large displacement model for membrane structures based on the combined finite-discrete element method (FDEM) has been developed. The model is implemented in the open source FDEM package - Yfdem. The paper also presents benchmark tests and numerical results.

Key words: *membrane, multiplicative decomposition, nonlinear analysis, finite-discrete element method*

1. Introduction

In mechanical terms, the membrane carries loads by axial tension only and has theoretically negligible resistance to bending. The use of membranes in architecture allows lightweight construction. Further, membranes have a wide application in electrical, biological, industrial and aerospace engineering.

By their nature, membranes often include large displacements and (depending on the material) finite strains. Analytical models have been developed for flat circular [7] [6] and square membranes [3] subjected to uniform pressure and concentrated forces. Both solutions are in the form of infinite series. The main problem with analytical solutions is their limited scope - they can be found only for specific problems.

Experimental studies of membranes evolved from soap film models to laboratory setups using different material models and full scale test. Recent experimental studies include [13], in which experimental wrinkling phenomena of membranes were examined, [20] the behaviour of pressurized cylinders was studied [22], [2] and [28] ballooning of membranes was investigated. Every experimental study is a very valuable tool for the verification of analytical and numerical models.

Numerical models are mostly based on the finite element method. The main element types are triangular and quadrilateral elements with various enchantments. The advantages of the use of triangular elements are simplicity of mesh generation and formulation simplicity. Quadrilateral elements are more difficult to automatically mesh, they are more sensitive to mesh distortions and require additional warping corrections, but have increased accuracy in

comparison to triangular elements. In [10], quadrilateral elements are used for the numerical form-finding and compared to the experimental setup. The investigation presented in [21] showed the use of triangular elements with different enchanted strain functions. A form-finding solution for a membrane using dynamic relaxation and viscous truss elements is introduced in [29]. Axisymmetric problems of membrane structures were analysed in [4] using 2D elements. Paper [5] investigates the use of area coordinates to reduce mesh sensitivity of the quadrilateral element grid. The finite element analysis of membrane wrinkling is researched in [12]. In [9], the procedure called Direct Core Congruential Formulation is presented for modelling the membrane behaviour. In addition to the experimental study in [20], the results of the numerical model are compared. In order to take large displacements (rotation and translation) into account, the so called co-rotational formulation is often adapted in the finite element formulation [28]. In recent years, full multiplicative decomposition formulations have been adopted for solids in 2D and 3D as well as for shells [8], [23-25], [27].

In this paper, an extension of the consistent multiplicative decomposition to membranes has been developed. In the first part of the paper, a detailed description of the algorithmic formulation is given. This is followed by benchmark tests and numerical examples. Advanced nonlinear material formulations are outside of the scope of this paper.

2. FDEM membrane model based on 3-noded finite element

The FDEM uses an explicit central difference integration scheme to resolve equations of motion directly. This is combined with lumped nodal masses, meaning that there is no need for either stiffness or mass matrices to be assembled. At each time step for each finite element, nodal forces are calculated from the current nodal displacements, see [14] and [16] and [15],[17],[18],[30] and [31]. For the static problem, the dynamic relaxation is employed.

The damping procedure is done according to [19]. The so-called $M(M^{-1}K)^m$ procedure is implemented in the central difference integration method. This type of the damping method attenuates both, high and low frequencies, and the processing time is shorter. This method also has a very little effect on the integration stability when compared to the undamped system.

For the sake of simplicity and efficiency, the simplest 3-noded triangle in 3D has been adopted. The geometry of the triangle is defined by three nodes, as shown in Fig 1.

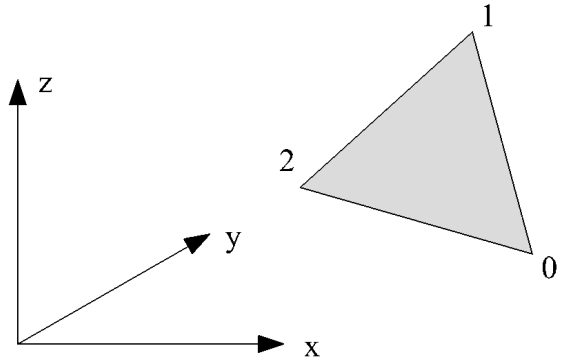

Fig. 1 Geometry of the constant strain triangle finite element

Each of the nodes is described by its Cartesian coordinates (*x,y,z*), where $(\bar{x},\bar{y},\bar{z})$ represent local initial Cartesian coordinates and $(\tilde{x},\tilde{y},\tilde{z})$ represent local current Cartesian coordinates, as shown in Fig 2.

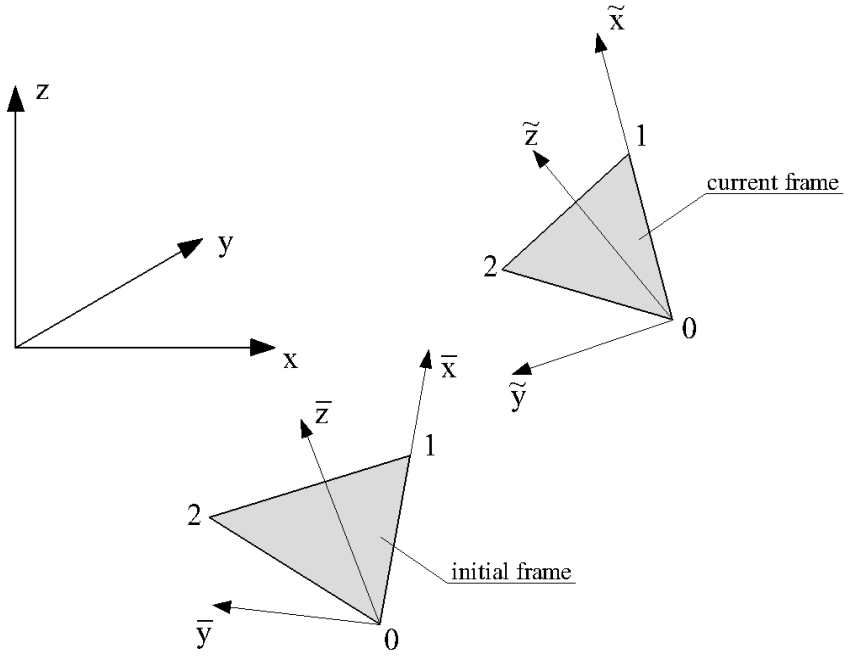

Fig. 2 Initial and current coordinates of the nodes of the finite element

In order to speed up the calculations, nodal coordinates are transformed from a global 3D to a local 2D coordinate system. The deformation gradient **F** is given by

$$\mathbf{F} = \begin{bmatrix} \tilde{x}_1 - \tilde{x}_0 & \tilde{x}_2 - \tilde{x}_0 \\ \tilde{y}_1 - \tilde{y}_0 & \tilde{y}_2 - \tilde{y}_0 \end{bmatrix} \begin{bmatrix} \bar{x}_1 - \bar{x}_0 & \bar{x}_2 - \bar{x}_0 \\ \bar{y}_1 - \bar{y}_0 & \bar{y}_2 - \bar{y}_0 \end{bmatrix}^{-1} \tag{1}$$

Since the origin of local coordinate systems coincides with the first node of the element, **F** can be written as

$$\mathbf{F} = \begin{bmatrix} \tilde{x}_1 & \tilde{x}_2 \\ \tilde{y}_1 & \tilde{y}_2 \end{bmatrix} \begin{bmatrix} \bar{x}_1 & \bar{x}_2 \\ \bar{y}_1 & \bar{y}_2 \end{bmatrix}^{-1} \tag{2}$$

which trivialises the calculation of the deformation gradient, resulting in the ultra-fast calculation, while preserving the consistent multiplicative decomposition.

Green-St. Venant strain tensor is obtained from **F**

$$\mathbf{E} = \frac{1}{2}(\mathbf{F}\mathbf{F}^{\mathrm{T}} - \mathbf{I}) \tag{3}$$

By employing a constitutive law depending on the material, the Cauchy stress tensor **T** is derived. Traction forces along the element edge can be written as

$$\begin{bmatrix} f_{\tilde{x}} \\ f_{\tilde{y}} \end{bmatrix} = \mathbf{T} \begin{bmatrix} m_{\tilde{x}} \\ m_{\tilde{y}} \end{bmatrix} \tag{4}$$

where $m_{\tilde{x}}$ and $m_{\tilde{y}}$ present components of the normal along the edge of the finite element. Each node takes half of the traction forces from neighbouring sides of the finite element. Since **T** is calculated in the corresponding local Cartesian coordinate system, the obtained nodal forces are then transformed into the global coordinate system and added to the global force vector.

Pretensioning stresses can be considered by adjusting the initial geometry of the membrane. In order to cause additional tension, the membrane in its initial frame represents a form of membrane without any external loading. By restraining it to boundary conditions and loading, membrane current stresses are calculated in comparison to the unloaded state. This is suitable for defining an optimal form of the membrane in certain boundary conditions and loading.

3. Validation and verification

Circular membrane under concentrated load. The first example is a circular membrane with rigidly clamped boundary conditions, subjected to the concentrated force in its centre. Characteristics of the given example are: radius of a membrane a=2m, Young's modulus multiplied by the membrane thickness Eh= 20000 N/m', Poisson's ratio ν = 0 and force P = 1 N. The numerical analyses are performed by using four different mesh densities, as shown in Fig. 3. Mesh densities are as follows: the first mesh (M1) has 352 elements, the second (M2) has 1216 elements, the third (M3) has 2208 elements, and the fourth (M4) is the finest mesh with 3968 elements. Figure 3 also shows the von Mises stress distributions. Perspective views of membrane deformations with displacements scaled by a factor of 25 are shown in Fig. 4.

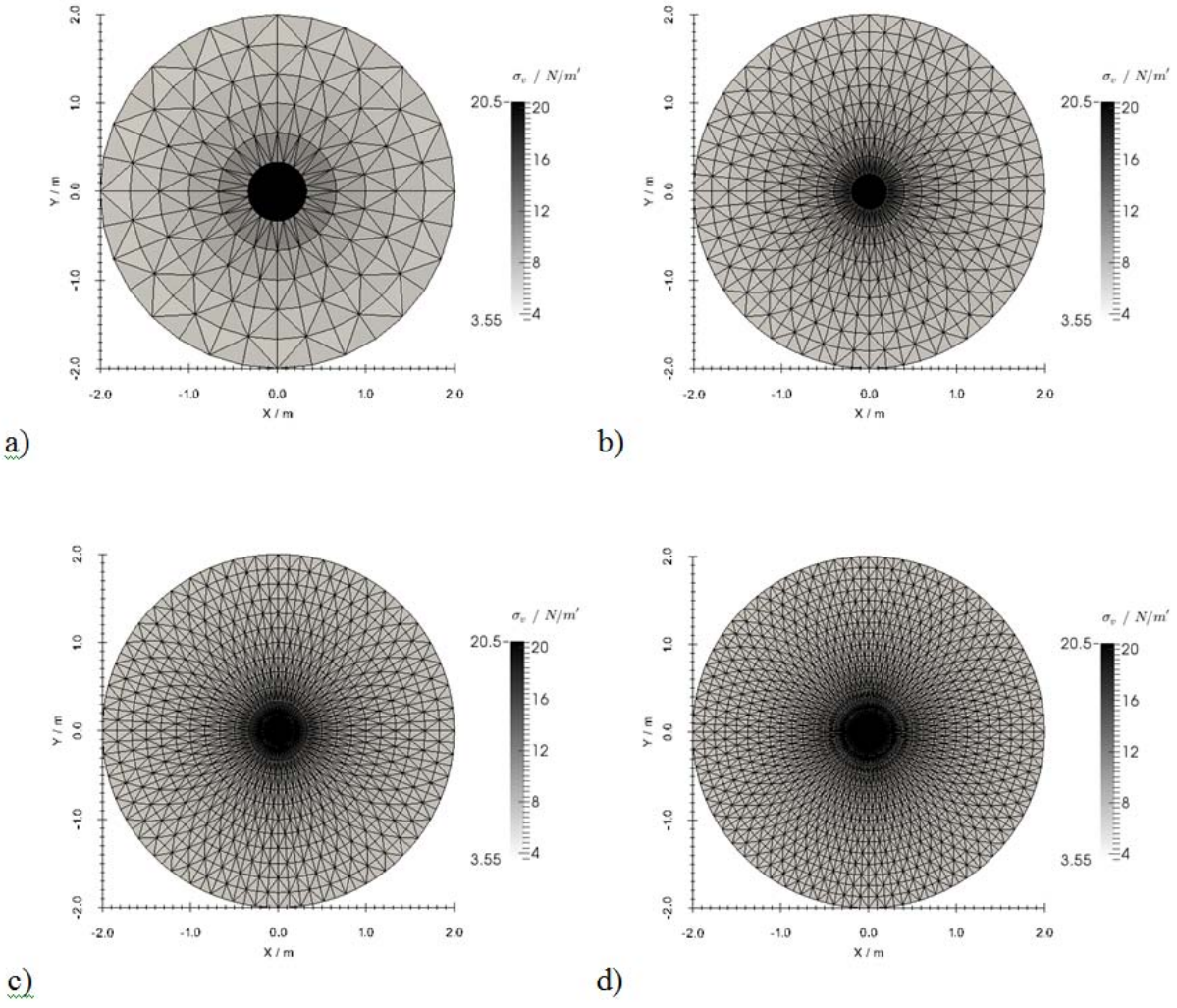

Fig. 3 Von Mises stress distribution a) M1, b) M2, c) M3, d) M4

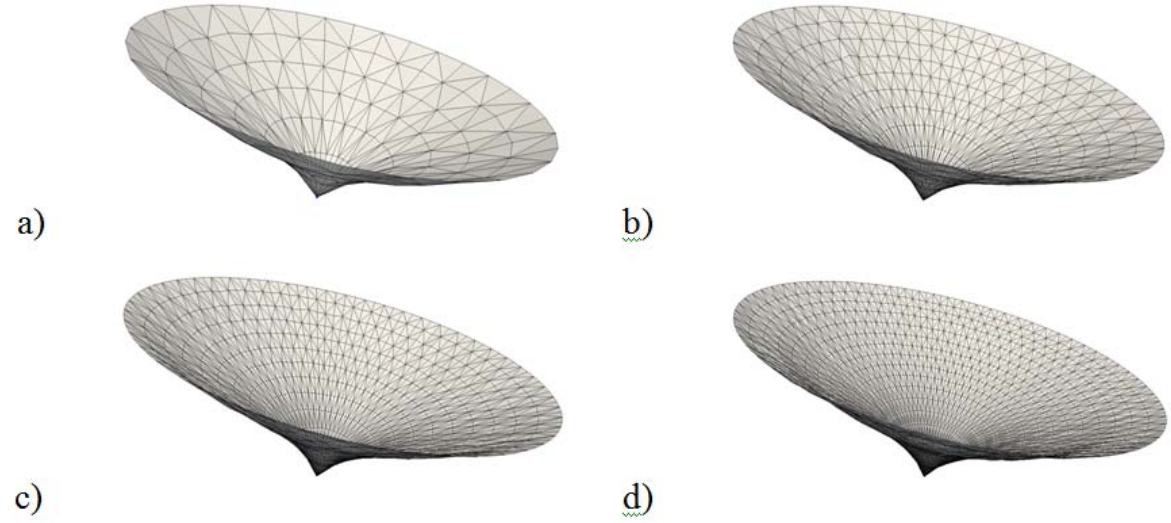

Fig. 4 Deformed membrane for a) M1, b) M2, c) M3, d) M4

An analytical solution for the displacement of flat circular membranes subjected to concentrated force is given by

$$w_0 = \sqrt[3]{\frac{4a^2 g(\nu) P_0}{\pi E h}} \tag{5}$$

where a is the radius of the membrane, P_o is the concentrated force, E is Young's modulus, h is the membrane thickness and $g(\nu)$ is the function depending on Poisson's ratio ν and angle θ_m, see [6] . $g(\nu)$ is calculated by obtaining θ_m from the equation $\nu=\nu(\theta_m)$, and then applying both in the expression for g. If $0<\nu<1/3$, values for θ_m and g are given by

$$\begin{aligned} \nu &= \frac{\cos\theta_m}{\sin^3\theta_m}(2\theta_m - \sin(2\theta_m)) - 1 \\ g &= \frac{1}{(1+\nu)} \frac{{\theta_m}^3 \cos\theta_m}{\sin^3\theta_m} \end{aligned} \tag{6}$$

if $1/3<\nu<1/2$, values for θ_m and g are given by

$$\begin{aligned} \nu &= \frac{2\left[\cos\theta_m - \sin^2\theta_m \ln(\cot(\frac{\theta_m}{2}))\right]}{\cos^3\theta_m} - 1 \\ g &= -\frac{1}{(1+\nu)} \frac{\sin^2\theta_m}{\cos^3\theta_m} \ln^3\left|\frac{1}{\sin\theta_m} - \frac{\cos\theta_m}{\sin\theta_m}\right| \end{aligned} \tag{7}$$

and if $\nu=1/3$, g equals 3/4.

The displacement obtained by using the presented numerical model is compared with that predicted by [6], and the results are shown in Fig 5. It can be seen that the numerical model, with the increase in the number of finite elements, converges to the analytical solution.

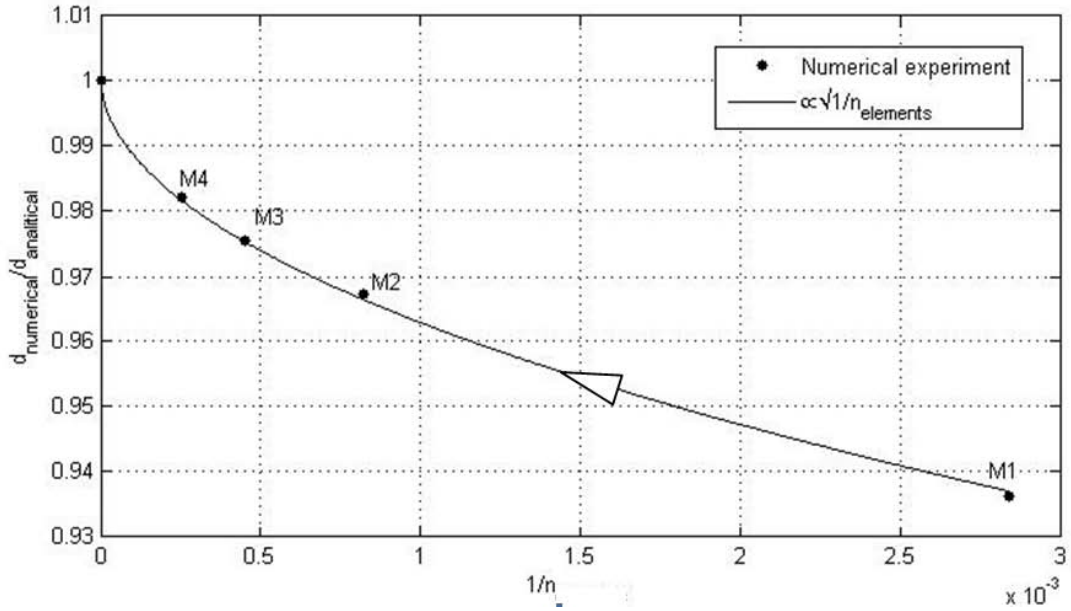

Fig. 5 Convergence of the numerical model

Membrane strip subjected to gravitational load. A membrane strip supported on shorter edges and subjected to gravitational load has been analysed. The membrane, in its unstrained state, has dimensions of 2 meters in width by 24 meters in length. The material characteristics are: elasticity, the Lame constants multiplied by membrane thickness (h=0.001m) λh = 52.1 kN/m and μh=56.4 kN/m. The mass of the membrane is m=10kg/m^2. Numerical analyses are performed by using the mesh density of 3072 elements. The perspective view of membrane displacements within the presented numerical model can be seen in Fig. 6.

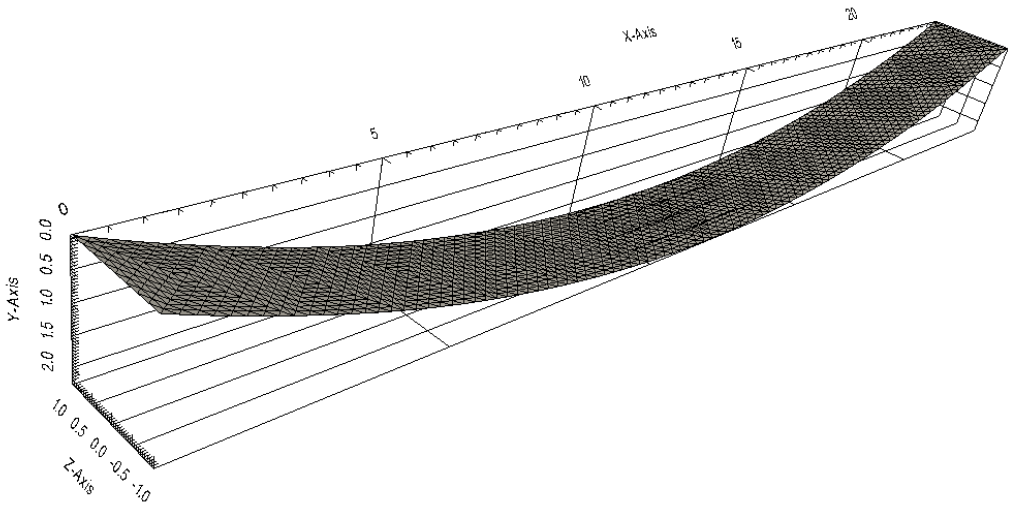

Fig. 6 Membrane geometry at rest

Membrane displacement in this configuration is analogue to the response of an elastic catenary with the same boundary conditions. An analytical solution for the catenary suspended between two supports is given in parametric equations, over parameter *s* that denotes the length of the unstretched catenary.

$$
\begin{aligned}
x(s) &= \frac{Hs}{EA} + \frac{HL_o}{W} \cdot \left[\sinh^{-1}\left(\frac{V}{H}\right) - \sinh^{-1}\left(\frac{V - Ws/L_o}{H}\right) \right] \\
y(s) &= \frac{Ws}{EA} \cdot \left(\frac{V}{W} - \frac{s}{2L_0}\right) + \frac{HL_0}{W} \left\{ \left[1 + \left(\frac{V}{H}\right)^2 \right]^{0.5} - \left[1 + \left(\frac{V - Ws/L_0}{H}\right)^2 \right]^{0.5} \right\} \\
T(s) &= \left[H^2 + \left(V - W\frac{s}{L_0} \right)^2 \right]^{0.5} \\
W &= \rho g L_0
\end{aligned}
\tag{8}
$$

where x(s) is the *x* coordinate of the catenary, y(s) is the y coordinate of the catenary, H and V are horizontal and vertical forces at the support, E is Young's modulus, A is the area of the cross section of the catenary, T is tension along the catenary, L_0 is the unstrained length of the catenary, ρ is unit weight per length of the unstrained catenary and g is the gravitational constant [11]. For the stated parameters, the analytical solution yields the maximum displacement of 2.2531 m in the middle of the span, with maximum tension being 3380.5 kN at the supports. It can be seen that the presented numerical model can accurately predict the behaviour of the membrane, with the maximum displacement difference of 1.41%.

4. Numerical examples

Form-finding application. Initially, a flat rectangular membrane with dimensions of 24 cm × 15 cm (Fig. 7) is subjected to the vertical displacement of 3.2 cm in the middle of its longer sides, i.e. the longer edge of the support has new boundary conditions with the middle point being 3.2 cm below the corners of the supports (Fig. 8). This type of support forces the membrane with the initially flat geometry into the saddle shape. The material characteristics are: the Lame constants multiplied by the membrane thickness (*h*=0.001m) λh = 5210 kN/m and μh=5640 kN/m. The mass of the membrane is m=20 kg/m2. Numerical analyses are performed by using the mesh density of 4096 elements (Fig. 7). Von Mises stress distributions and the perspective view of the deformed membrane are shown in Fig 8. This example could also be solved by numerically solving the partial differential equation (PDE) of minimal surface with corresponding boundary conditions.

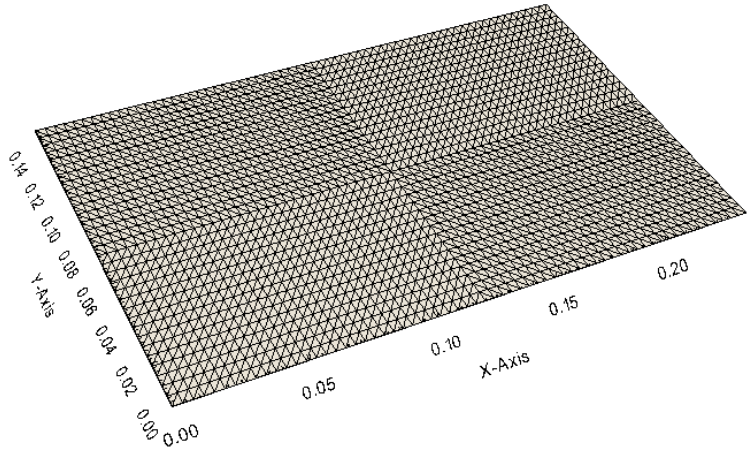

Fig. 7 Initial geometry and mesh density

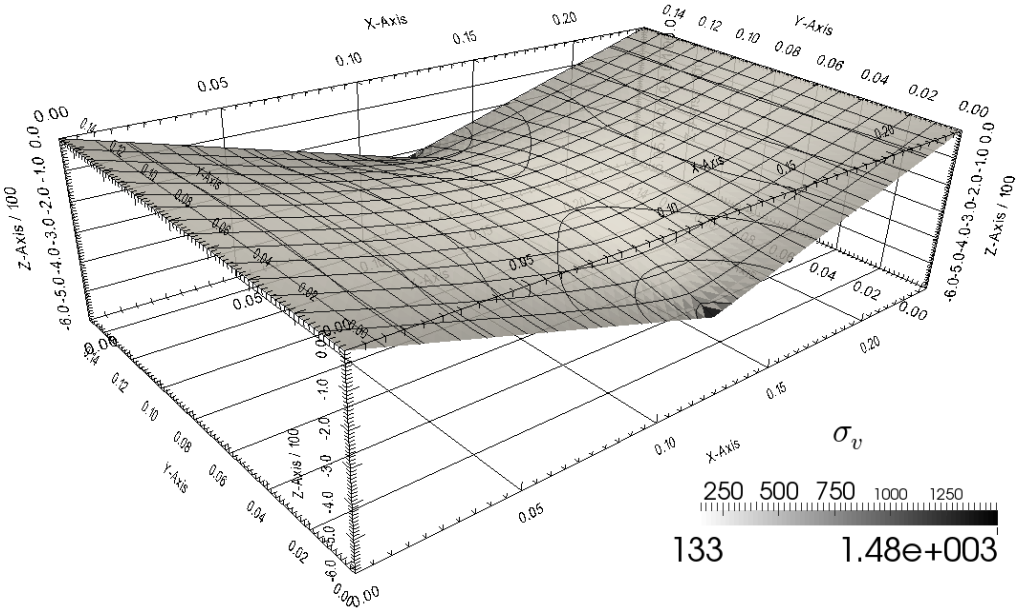

Fig. 8 Von Mises stress distribution

Influence of initial geometry of membrane. The same example as the above one is presented with two different initial geometries. In the first example, the initial membrane geometry is 20% longer in the y direction (24 cm × 18 cm) and in the second example, the initial membrane geometry is 20 % shorter in the y direction (24 cm × 12 cm). The material characteristics, loading and boundary conditions are the same as in the previous example. Numerical analyses are performed by using mesh roughness with 4096 elements, as shown in Fig. 9. Figures 10 and 11 show the von Mises stress distributions and a perspective view of the deformed membrane, i.e. of the 20% longer (Fig 10) and 20% shorter membrane (Fig 11). It can be seen that the proposed numerical model describes wrinkling effects in the case of the initially longer membrane, since the membrane is not able to carry the compression forces. In the case of the initial geometry of 24 cm × 12 cm, additional tensioning occurs, which results in smaller displacements compared to the previous example. It should be noted that in the case of the wrinkling effects, the classical approach based on PDE and minimal surface is not applicable.

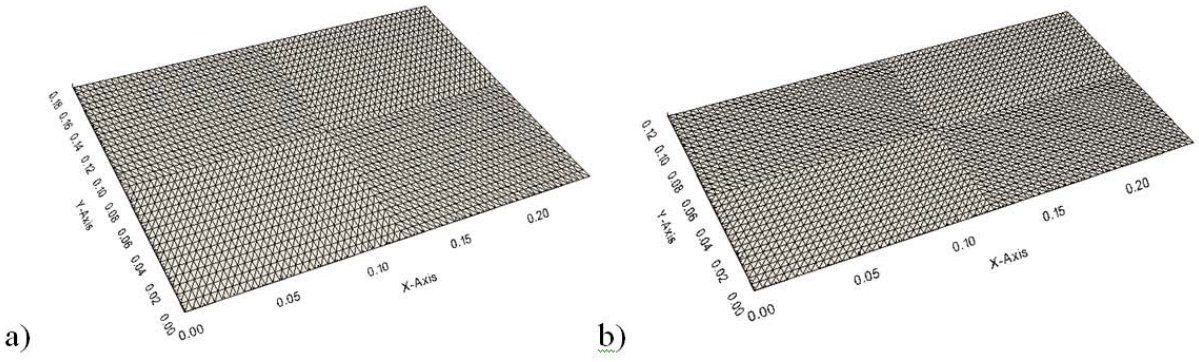

Fig. 9 Initial geometry for a) longer membrane b) shorter membrane

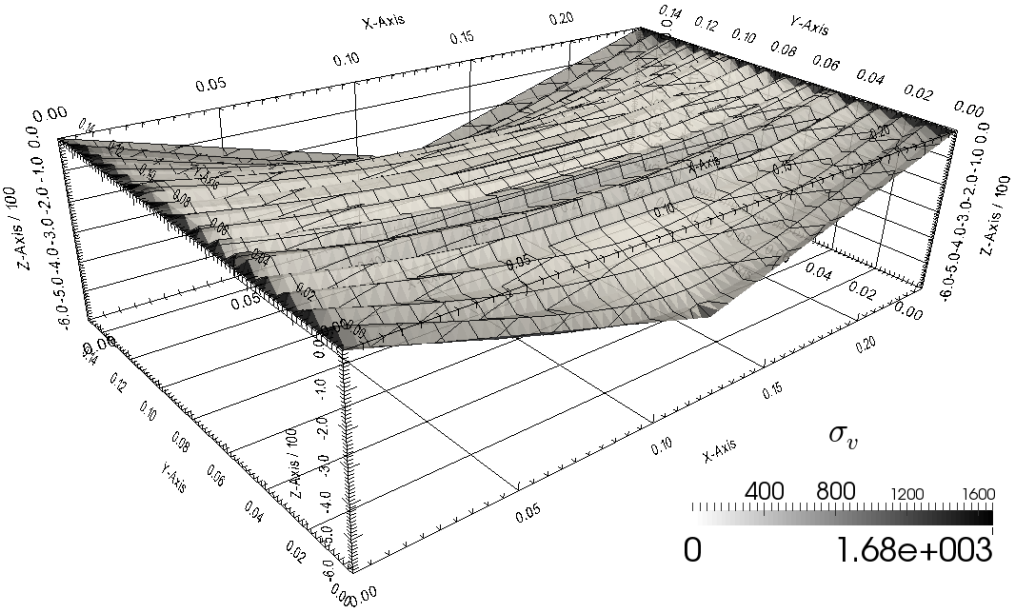

Fig. 10 Von Mises stress distribution for initially longer membrane

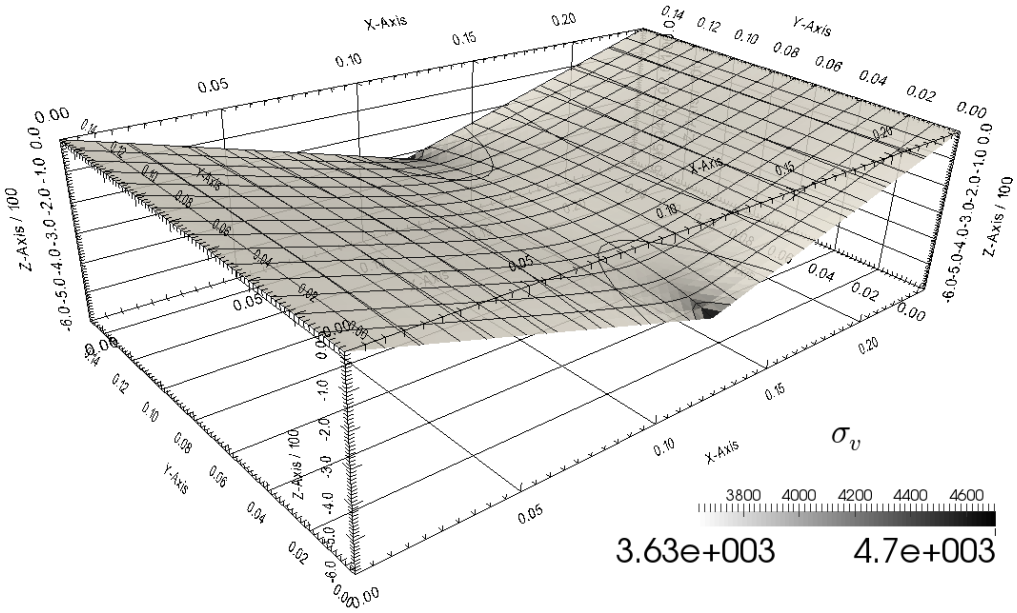

Fig. 11 Von Mises stress distribution for initially shorter membrane

Stress concentration in elastic analysis. A square membrane with dimensions of 2 m × 2 m and a circular hole of 0.1 m in radius in the middle is analysed. The membrane is supported at two opposite edges and subjected to uniform pressure of p=1000 N/m^2. The material characteristics are: the Lame constants multiplied by the membrane thickness (h=0.001m) λh = 446 kN/m and μh= 396 kN/m. The mass of the membrane is m=0.25 kg/m^2. Figure 12 shows the discretization of the problem and stress distribution for σ_y. Figure 13 shows a perspective view of the deformed membrane and stress distribution for σ_y. Distributions of σ_x and σ_y stresses along the x axis (y=0) are shown in Fig. 14. An analytical solution for the nominal stress is given by [32]

$$\sigma_{nom} = \frac{P}{h(D-d)} \tag{9}$$

where d equals the diameter of the hole and D equals half of the distance between the centre of the hole and the sides of the square. Maximum stresses along the edge of the circular hole σ_{max} can be written as

$$\sigma_{\max} = K_t \cdot \sigma_{nom} \tag{10}$$

where K_t is the static stress concentration factor in the elastic range given by [32]

$$K_t = 3 - 3.140 \cdot \left(d/D\right) + 3.667 \cdot \left(d/D\right)^2 - 1.527\left(d/D\right)^3 \tag{11}$$

In this example, K_t=2.721. The here presented numerical model calculates K_t=2.667, which is 2% difference when compared to the analytical solution.

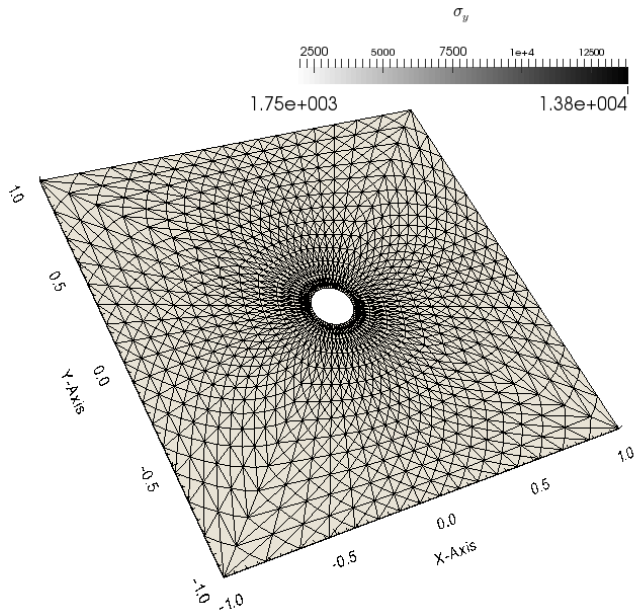

Fig. 12 Discretisation and stress distribution

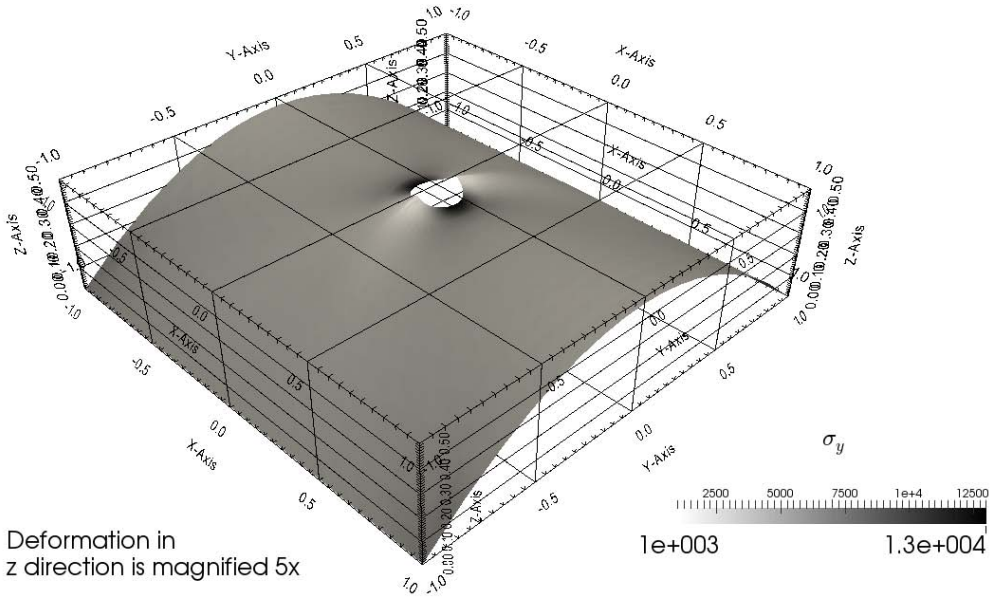

Fig. 13 Deformation of the membrane with stress distribution

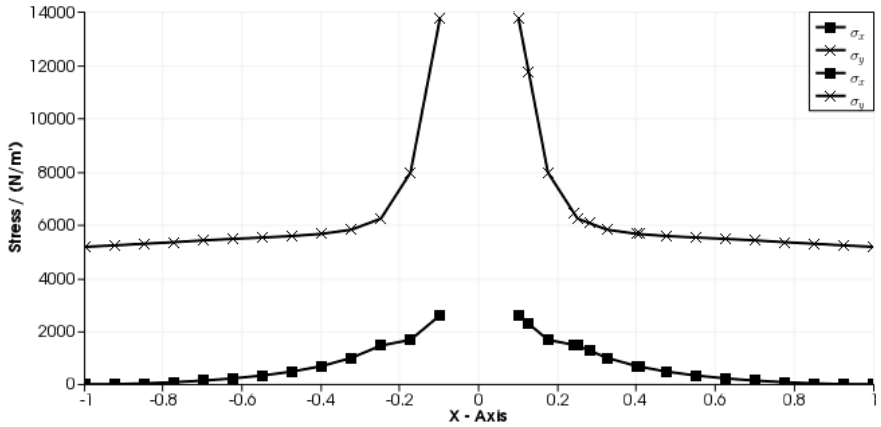

Fig. 14 Stress distribution along the *x* axis (*y*=0)

5. Conclusion

This paper presents a new numerical model for the analysis of membrane structures under static loads. It is based on the existing FDEM Y code with a new finite element and a new procedure for implementing pretension. The advantages of the presented model are its ability to handle both large displacements and large rotations on arbitrary shaped membranes under arbitrary static loads. The verification examples demonstrate that the results obtained by the presented numerical model are accurate compared to the analytical solutions. The results converge to the analytical solutions at the rate of $\sqrt{n}$, with n being the number of finite elements. As shown in the form-finding examples, by the manipulation of the initial geometry, various shapes of the membrane can be obtained with the same boundary conditions. This property is used for investigating optimal cutting shapes. Using the $M(M^{-1}K)^m$ damping method, the presented FDEM numerical model is suitable for predicting the behaviour of membrane structures when subjected to static loads.

Further work is needed to demonstrate material nonlinearity and/or fracture together with contact and folding.

REFERENCES

[1] Bangash, T., Munjiza, A., (2003) *Experimental validation of a computationally efficient beam element for combined finite-discrete element modelling of structures in distress*, Computational Mechanics, 30 (5-6), pp. 366-373.

[2] Baskaran, A., Murty, B., & Wu, J. (2009) *Calculating roof membrane deformation under simulated moderate wind uplift pressures,* Engineering Structures, 31 (3), 642-650.

[3] Bouzidi, R., Le Van, A., (2004) *Numerical solution of hyperelastic membranes by energy minimization*, Computers and Structures, 82 (23-26), 1961-1969.

[4] Bouzidi, R., Ravaut, Y., Wielgosz, C. (2003) *Finite elements for 2D problems of pressurized membranes*, Computers and Structures, 81 (26-27), 2479-2490.

[5] Chen, X.-M., Cen, S., Long, Y.-Q., Yao, Z.-H., (2004) *Membrane elements insensitive to distortion using the quadrilateral area coordinate method*, Computers and Structures, 82 (1), 35-54.

[6] Cong-rui, J. (2008) *Large deflection of circular membrane under concentrated force*, Applied Mathematics and Mechanics, Engl. Ed., 29(7), 889–896.

[7] Fichter, W. B., (1997) *Some Solutions for the Large Deflections of Uniformly Loaded Circular Membranes*, Hampton, Virginia, NASA.

[8] Fox, D.D., Simo, J.C., (1992) *A drill rotation formulation for geometrically exact shells*, Computer Methods in Applied Mechanics and Engineering, 98 (3), pp. 329-343.

[9] Gil, A., (2006) *Structural analysis of prestressed Saint Venant-Kirchhoff hyperelastic membranes subjected to moderate strains*, Computers and Structures, 84 (15-16), 1012-1028.

[10] Gosling, P., Lewis, W., (1996) *Optimal structural membranes - II. Form-finding of prestressed membranes using a curved quadrilateral finite element for surface definition*, Computers and Structures, 61 (5), 885-895.

[11] Irvine, M., (1992) *Cable Structures,* Dover Publications Inc.

[12] Lee, E.-S., Youn, S.-K., (2006) *Finite element analysis of wrinkling membrane structures with large deformations*, Finite Elements in Analysis and Design, 42 (8-9), 780-791.

[13] Miyamura, T., (2000) *Wrinkling on stretched circular membrane under in-plane torsion: Bifurcation analyses and experiments*, Engineering Structures, 22 (11), 1407-1425.

[14] Munjiza, A., (2004) *The Combined Finite-Discrete Element Method*, John Wiley & Sons.

[15] Munjiza, A., John, N.W.M., (2001) *Mesh size sensitivity of the combined FEM/DEM fracture and fragmentation algorithms*, Engineering Fracture Mechanics, 69 (2), pp. 281-295.

[16] Munjiza, A.A., Knight, E.E., Rougier, E., (2011) *Computational Mechanics of Discontinua*, Wiley

[17] Munjiza, A., Latham, J.-P., (2004*) Some computational and algorithmic developments in computational mechanics of discontinua*, Philosophical Transactions of the Royal Society A: Mathematical, Physical and Engineering Sciences, 362 (1822), pp. 1817-1833.

[18] Munjiza, A., Owen, D.R.J., Bicanic, N., (1995) *Combined finite-discrete element method in transient dynamics of fracturing solids*, Engineering computations, 12 (2), pp. 145-174.

[19] Munjiza A., Owen D. R. J., Crook A. J. L., (1998) An $M(M^{-1}K)^m$ proportional damping in explicit integration of dynamic structural systems, International journal for numerical methods in engineering, Vol. 41, 1277-1296

[20] Pamplona, D., Gonalves, P., Lopes, S., (2006) *Finite deformations of cylindrical membrane under internal pressure*, International Journal of Mechanical Sciences, 48 (6), 683-696.

[21] Piltner, R., Taylor, R., (2000) *Triangular finite elements with rotational degrees of freedom and enhanced strain modes*, Computers and Structures, 75 (4), 361-368.

[22] Shi, X., Burnett, E., (2008) *Mechanics and test study of flexible membranes ballooning in three dimensions*, Building and Environment, 43 (11), 1871-1881.

[23] Simo, J.C., (1998) *Numerical analysis and simulation of plasticity*, Handbook of Numerical Analysis, 6, pp. 183-499.

[24] Simo, J.C., (1993) *On a stress resultant geometrically exact shell model. Part VII: Shell intersections with 5 6-DOF finite element formulations*, Computer Methods in Applied Mechanics and Engineering, 108 (3-4), pp. 319-339.

[25] Simo, J.C., Tarnow, N., (1994) *New energy and momentum conserving algorithm for the non-linear dynamics of shells*, International Journal for Numerical Methods in Engineering, 37 (15), pp. 2527-2549.

[26] Smoljanović, H., Živaljić, N., Nikolić, Ž., (2013) *A combined finite-discrete element analysis of dry stone masonry structures*, Engineering structures. 52, 89-100.

[27] Taylor, R.L., Simo, J.C., (1985) *Bending and membrane elements for analysis of thick and thin shells*, NUMETA 85, Numerical Methods in Engineering: Theory and Applications, Proceedings of the International Conference, Swansea, Wales pp. 587-591.

[28] Wang, S., Liu, G., Zhang, Z., Chen, L., (2011) *Nonlinear 3D numerical computations for the square membrane versus experimental data*, Engineering Structures, 33 (5), 1828-1837.

[29] Wood, R. D., (2002) *A simple technique for controlling element distortion in dynamic relaxation form finding of tension membranes*, Computers and Structures (80), 2115-2120.

[30] Xiang, J., Munjiza, A., Latham, J.-P., (2009) *Finite strain, finite rotation quadratic tetrahedral element for the combined finite-discrete element method*, International Journal for Numerical Methods in Engineering, 79 (8), pp. 946-978.

[31] Xiang, J., Munjiza, A., Latham, J.-P., Guises, R., (2009) *On the validation of DEM and FEM/DEM models in 2D and 3D*, Engineering Computations (Swansea, Wales), 26 (6), pp. 673-687.

[32] Young, W. C., Budynas, R. G., (2001) *Roark's Formulas for Stress and Strain*, McGraw-Hill Companies.

[33] Živaljić, N.; Smoljanović, H.; Nikolić, Ž., (2013) *A combined finite-discrete element model for RC structures under dynamic loading*, Engineering computations, Vol 30, 7; 982-1010.

Submitted: 27.8.2013

Accepted: 06.3.2014

Vladimir Divić
Ivana Uzelac
Bernardin Peroš
Faculty of Civil Engineering, Architecture and Geodesy, University of Split
Matice hrvatske 15
21000 Split